

A normal form for Hamiltonian-Hopf bifurcations in generalized nonlinear Schrödinger equations

Jianke Yang
Department of Mathematics and Statistics
University of Vermont
Burlington, VT 05401, USA

Abstract

A normal form is derived for Hamiltonian-Hopf bifurcations of solitary waves in generalized nonlinear Schrödinger equations. This normal form is a simple second-order nonlinear ordinary differential equation that is asymptotically accurate in describing solution dynamics near Hamiltonian-Hopf bifurcations. When the nonlinear coefficient in this normal form is complex, which occurs if the second harmonic of the Hopf bifurcation frequency falls inside the continuous spectrum of the system, the solution of this normal form will blow up to infinity in finite time, meaning that solution oscillations near Hamiltonian-Hopf bifurcations will strongly amplify and eventually get destroyed. When the nonlinear coefficient of the normal form is real, the normal form can admit periodic solutions, which correspond to long-lasting solution oscillations in the original PDE system. Quantitative comparison between the normal form's predictions and true PDE solutions is also made in several numerical examples, and good agreement is obtained.

1 Introduction

Bifurcations of stationary waves are common phenomena in both conservative and dissipative nonlinear wave systems (see [1, 2, 3, 4, 5, 6, 7, 8, 9, 10, 11, 12, 13, 14, 15, 16, 17, 18, 19, 20] for instance). Notable examples include symmetry-breaking bifurcations, fold bifurcations, Hopf bifurcations and period-doubling bifurcations, all of which have counterparts in dynamical systems. Bifurcations of stationary waves induce qualitative changes to the wave behavior and can be used to control system outcome, thus their studies are both mathematically and physically important.

Hamiltonian-Hopf bifurcations occur in conservative wave systems, where pairs of imaginary eigenvalues in the linear-stability spectrum of stationary

waves coalesce and then move off the imaginary axis, creating oscillatory instability. These linear instabilities have been well analyzed, and it has been shown that only collisions of imaginary eigenvalues with opposite Krein signatures can induce such bifurcations [21, 22, 23]. However, nonlinear wave dynamics near such bifurcations is less known. One step in this direction was made by Goodman [15], where Hamiltonian-Hopf bifurcations of solitary waves were examined in the nonlinear Schrödinger (NLS) equation with potentials of primarily symmetric triple-well type. Projecting the solution to three linear eigenmodes of the potential and making a Galerkin truncation and symmetry reduction, a Hamiltonian system of ordinary differential equations (ODEs) for two complex variables was derived. Numerical simulations of this ODE model showed oscillatory as well as chaotic solutions at different power levels, which resemble dynamics in the original PDE system. However, this analysis is only suitable to Hamiltonian-Hopf bifurcations at low powers of solitons, where the solution projection onto linear modes is justified (at higher soliton powers, the error of Galerkin truncation will be significant). In addition, the derived ODE model is complicated, which hinders analytical predictions of ODE dynamics. Furthermore, the resonant effect of higher harmonics of solution oscillations with the continuous spectrum is invisible in this analysis.

In this paper, we derive a normal form for general Hamiltonian-Hopf bifurcations of solitary waves (solitons) in NLS equations with arbitrary external potentials. This normal form is a simple second-order nonlinear ODE. It is derived near a Hamiltonian-Hopf bifurcation point by multi-scale perturbation methods and is asymptotically accurate in describing solution dynamics near Hamiltonian-Hopf bifurcations. When the nonlinear coefficient in this normal form is complex, which occurs if the second harmonic of the Hopf bifurcation frequency is resonant with the continuous spectrum of the system, the solution of this normal form will blow up to infinity in finite time, meaning that solution oscillations near Hamiltonian-Hopf bifurcations will strongly amplify and eventually get destroyed. When the nonlinear coefficient of the normal form is real, the normal form can admit periodic solutions, which correspond to long-lasting solution oscillations in the original PDE system. Quantitative comparison between the normal form's predictions and true PDE solutions is also made in several numerical examples, and good agreement is obtained.

2 Analytical conditions for Hamiltonian-Hopf bifurcations

We consider the NLS equation with a general external potential,

$$iU_t + U_{xx} - V(x)U + \sigma|U|^2U = 0, \quad (1)$$

where $V(x)$ is a real-valued localized potential function, and $\sigma = \pm 1$ is the sign of nonlinearity. This equation models nonlinear light propagation in a Kerr medium under paraxial approximation, as well as dynamics of Bose-Einstein

condensates under mean-field approximation [24, 25, 26]. Eq. (1) is a Hamiltonian system. Note that the cubic nonlinearity and localized linear potential in this model are chosen primarily for convenience, as the analysis to be developed in this article can be readily extended to arbitrary forms of nonlinearities and potentials [19].

Solitons in Eq. (1) have the form

$$U(x, t) = e^{i\mu t} u(x), \quad (2)$$

where $u(x)$ is a real-valued localized function solving the equation

$$u_{xx} - \mu u - V(x)u + \sigma u^3 = 0, \quad (3)$$

and μ is a real-valued propagation constant. These solitons exist as continuous families parameterized by μ . Since the potential $V(x)$ is localized, μ is positive for all these solitons.

Linear stability of these solitons is determined by substituting the normal-mode perturbation

$$U(x, t) = e^{i\mu t} \left[u(x) + f_1(x)e^{\lambda t} + f_2^*(x)e^{\lambda^* t} \right], \quad f_1, f_2 \ll 1 \quad (4)$$

into Eq. (1), which leads to the following linear eigenvalue problem

$$iL \begin{bmatrix} f_1 \\ f_2 \end{bmatrix} = \lambda \begin{bmatrix} f_1 \\ f_2 \end{bmatrix}, \quad (5)$$

where

$$L = \begin{bmatrix} \partial_{xx} - \mu - V + 2\sigma u^2 & \sigma u^2 \\ -\sigma u^2 & -(\partial_{xx} - \mu - V + 2\sigma u^2) \end{bmatrix}, \quad (6)$$

λ is the eigenvalue, and the superscript ** represents complex conjugation. Notice that $\sigma_3 L$ is a self-adjoint operator, where $\sigma_3 = \text{diag}(1, -1)$ is the third Pauli-spin matrix. That is, $(\sigma_3 L)^A = \sigma_3 L$, with the superscript A representing the adjoint of an operator. Thus

$$L^A = \sigma_3 L \sigma_3. \quad (7)$$

It is easy to see that if λ is an eigenvalue of iL , so are λ^* , $-\lambda$ and $-\lambda^*$. Thus purely-real and purely-imaginary eigenvalues appear as $\pm\lambda$ pairs, and other eigenvalues appear as quadruples. If all eigenvalues λ lie on the imaginary axis, then the soliton (2) is linearly stable; otherwise it is linearly unstable.

Hamiltonian-Hopf bifurcations of solitons occur when pairs of eigenvalues on the imaginary axis collide and move off the imaginary axis, creating linear oscillatory instability. Suppose this Hamiltonian-Hopf bifurcation occurs at the soliton with $\mu = \mu_0 > 0$, eigenvalues collide at $\lambda = \pm i\omega$ on the imaginary axis (with $\omega > 0$ being the Hopf frequency), and $i\omega$ is a double eigenvalue of iL_0 , where $L_0 \equiv L|_{\mu=\mu_0}$. Then the condition for this bifurcation is that the geometric multiplicity of $i\omega$ is one (less than its algebraic multiplicity two). In

other words, the double eigenvalue $i\omega$ of iL_0 admits a single eigenfunction and a generalized eigenfunction. More explicitly, there exist a single real eigenfunction $[\psi_1, \psi_2]^T$ and a generalized real eigenfunction $[\phi_1, \phi_2]^T$ such that

$$L_0 \begin{bmatrix} \psi_1 \\ \psi_2 \end{bmatrix} = \omega \begin{bmatrix} \psi_1 \\ \psi_2 \end{bmatrix}, \quad (8)$$

$$(L_0 - \omega) \begin{bmatrix} \phi_1 \\ \phi_2 \end{bmatrix} = \begin{bmatrix} \psi_1 \\ \psi_2 \end{bmatrix}, \quad (9)$$

and no higher generalized eigenfunctions exist, i.e., the equation

$$(L_0 - \omega) \begin{bmatrix} \chi_1 \\ \chi_2 \end{bmatrix} = \begin{bmatrix} \phi_1 \\ \phi_2 \end{bmatrix} \quad (10)$$

admits no solutions. Here the superscript ‘ T ’ represents transpose of a vector. In view of Eq. (7), we see that

$$(L_0 - \omega)^A \begin{bmatrix} \psi_1 \\ -\psi_2 \end{bmatrix} = 0, \quad (11)$$

i.e., $[\psi_1, -\psi_2]^T$ is in the kernel of $(L_0 - \omega)^A$. Hence in order for the generalized eigenfunction $[\phi_1, \phi_2]^T$ to exist in Eq. (9), the right hand side of this linear inhomogeneous equation must be orthogonal to the adjoint homogeneous solution $[\psi_1, -\psi_2]^T$, i.e.,

$$\int_{-\infty}^{\infty} (\psi_1^2 - \psi_2^2) dx = 0; \quad (12)$$

and in order for higher generalized eigenfunctions not to exist in Eq. (10), the right hand side of (10) must not be orthogonal to $[\psi_1, -\psi_2]^T$, i.e.,

$$\int_{-\infty}^{\infty} (\psi_1 \phi_1 - \psi_2 \phi_2) dx \neq 0. \quad (13)$$

Necessary conditions for Hamiltonian-Hopf bifurcations can also be formulated using Krein signatures of purely imaginary eigenvalues in the linear-stability operator iL [21, 23]. For a simple purely imaginary eigenvalue $\lambda = i\omega$ with real eigenfunction $F = [f_1, f_2]^T$, its Krein signature can be defined as

$$K_\lambda = \text{sgn} \langle -\sigma_3 L F, F \rangle = \text{sgn} \int_{-\infty}^{\infty} \omega (f_2^2 - f_1^2) dx, \quad (14)$$

where the inner product between two vector functions $f(x)$ and $g(x)$ is $\langle f, g \rangle = \int_{-\infty}^{\infty} f^{*T} g dx$. When two such eigenvalues collide on the imaginary axis, a necessary condition for Hamiltonian-Hopf bifurcations is that they have opposite Krein signatures. This necessary condition on Krein signatures is related to the conditions on eigenfunctions given above. Indeed, under conditions (12)-(13) for eigenfunctions, we can show that the purely imaginary eigenvalues before collision have opposite Krein signatures (details are omitted).

Regarding operator L_0 , it should be added that zero is its discrete eigenvalue since

$$L_0 \begin{bmatrix} u_0 \\ -u_0 \end{bmatrix} = 0. \quad (15)$$

In addition,

$$L_0^A \begin{bmatrix} u_0 \\ u_0 \end{bmatrix} = 0 \quad (16)$$

in view of Eq. (7). Furthermore, by differentiating the soliton equation (3) with respect to μ , we see that

$$L_0 \begin{bmatrix} u_{\mu 0} \\ u_{\mu 0} \end{bmatrix} = \begin{bmatrix} u_0 \\ -u_0 \end{bmatrix}, \quad (17)$$

where $u_{\mu 0}(x) \equiv u_\mu(x; \mu)|_{\mu=\mu_0}$. These relations will be used in later analysis.

In the next section, we will investigate solution dynamics near Hamiltonian-Hopf bifurcations. For that purpose, we make the following additional assumptions:

1. $2i\omega$ is not a discrete eigenvalue of iL_0 ;
2. Defining the linearization operator of the soliton equation (3) at $\mu = \mu_0$ as

$$M = \partial_{xx} - \mu_0 - V(x) + 3\sigma u_0^2, \quad (18)$$

we assume that the kernel of M is empty;

3. Defining the power of solitons $u(x; \mu)$ as

$$P(\mu) = \int_{-\infty}^{\infty} u^2(x; \mu) dx, \quad (19)$$

then we assume that $P'(\mu_0) \neq 0$.

The first assumption forbids nonlinearity-induced second-harmonic resonance of Hopf-bifurcation eigenmodes; the second assumption prohibits other potential bifurcations of solitons at this Hamiltonian-Hopf bifurcation point [19]; and the third assumption excludes additional linear instabilities [26]. These assumptions will be needed for our analysis to carry through.

3 A normal form for Hamiltonian-Hopf bifurcations

In this section, we derive an asymptotically accurate ODE model (a normal form) for wave dynamics near Hamiltonian-Hopf bifurcations. This normal form uses only information at the bifurcation point.

Near a Hamiltonian-Hopf bifurcation point $\mu = \mu_0$, the full PDE solution can be expanded into the following perturbation series,

$$U(x, t) = e^{i\theta} [u_0(x) + \epsilon U_1(x, t, T) + \epsilon^2 U_2(x, t, T) + \dots], \quad (20)$$

where

$$\theta(t, T) = \mu_0 t + \epsilon \int \mu_1(T) dT + \epsilon^2 \int \mu_2(T) dT + \dots, \quad (21)$$

$T = \epsilon t$, and $0 < \epsilon \ll 1$. Substituting this expansion into Eq. (1), the $O(1)$ equation is automatically satisfied. At $O(\epsilon)$, the equation for U_1 is found to be

$$(i\partial_t + \partial_{xx} - \mu_0 - V + 2\sigma u_0^2)U_1 + \sigma u_0^2 U_1^* = 0. \quad (22)$$

This equation can be rewritten as

$$(i\partial_t + L_0) \begin{bmatrix} U_1 \\ U_1^* \end{bmatrix} = 0. \quad (23)$$

In view of the conditions for Hamiltonian-Hopf bifurcations in Sec. 2, $i\omega$ is a double eigenvalue of iL_0 with a single real eigenfunction $[\psi_1, \psi_2]^T$. Due to eigenvalue symmetry, $-i\omega$ is also a double eigenvalue of iL_0 with a single real eigenfunction $[\psi_2, \psi_1]^T$. Thus the non-secular localized solution for U_1 is a slowly modulated Hopf oscillation mode

$$U_1 = B(T)\psi_1(x)e^{i\omega t} + B^*(T)\psi_2(x)e^{-i\omega t}, \quad (24)$$

where $B(T)$ is a complex envelope function to be determined.

At $O(\epsilon^2)$, the equation for U_2 is

$$\begin{aligned} & (i\partial_t + \partial_{xx} - \mu_0 - V + 2\sigma u_0^2)U_2 + \sigma u_0^2 U_2^* \\ & = \mu_1 u_0 - iU_{1T} - \sigma u_0 (2|U_1|^2 + U_1^2). \end{aligned} \quad (25)$$

When the U_1 -formula (24) is utilized, this U_2 equation becomes

$$\begin{aligned} & (i\partial_t + \partial_{xx} - \mu_0 - V + 2\sigma u_0^2)U_2 + \sigma u_0^2 U_2^* = \mu_1 u_0 \\ & - 2\sigma |B|^2 u_0 (\psi_1^2 + \psi_1 \psi_2 + \psi_2^2) - iB_T \psi_1 e^{i\omega t} - iB_T^* \psi_2 e^{-i\omega t} \\ & - \sigma B^2 u_0 (2\psi_1 \psi_2 + \psi_1^2) e^{2i\omega t} - \sigma B^{*2} u_0 (2\psi_1 \psi_2 + \psi_2^2) e^{-2i\omega t}. \end{aligned} \quad (26)$$

In view of Eqs. (9) and (17), the solution to this U_2 equation is

$$\begin{aligned} U_2 = & \mu_1 u_{\mu 0} - \sigma |B|^2 h - iB_T \phi_1 e^{i\omega t} + iB_T^* \phi_2 e^{-i\omega t} \\ & - \sigma B^2 g_1 e^{2i\omega t} - \sigma B^{*2} g_2^* e^{-2i\omega t}, \end{aligned} \quad (27)$$

where $h(x)$ is a real localized function defined by

$$h = M^{-1} [2u_0(\psi_1^2 + \psi_1 \psi_2 + \psi_2^2)], \quad (28)$$

$[\phi_1(x), \phi_2(x)]^T$ is the real generalized eigenfunction defined in (9), and $[g_1(x), g_2(x)]^T$ solves the equation

$$(L_0 - 2\omega) \begin{bmatrix} g_1 \\ g_2 \end{bmatrix} = \begin{bmatrix} u_0(2\psi_1\psi_2 + \psi_1^2) \\ -u_0(2\psi_1\psi_2 + \psi_2^2) \end{bmatrix}. \quad (29)$$

Note that the kernel of M is empty due to our second assumption in the end of Sec. 2, thus a localized real function $h(x)$ as defined in Eq. (28) exists and is unique.

An important remark is in order regarding the nature of the solution $[g_1, g_2]^T$ to Eq. (29), and this hinges on whether $2i\omega$ lies inside the continuous spectrum of the linear-stability operator iL_0 . Recall that the potential $V(x)$ is localized. Then for the soliton $u_0(x)$, the continuous spectrum of iL_0 is $i(-\infty, -\mu_0] \cup i[\mu_0, +\infty)$ on the imaginary axis.

(1) If $2i\omega$ does not lie in this continuous spectrum, meaning that $2\omega < \mu_0$, then in view of our first assumption in the end of Sec. 2, the kernel of $L_0 - 2\omega$ is empty, thus a localized real solution $[g_1, g_2]^T$ to Eq. (29) exists and is unique.

(2) If $2i\omega$ lies inside the continuous spectrum of iL_0 , i.e., $2\omega > \mu_0$, then resonance with the continuous spectrum occurs. In this case, the forcing term on the right side of Eq. (29) will excite continuous-wave radiation, which appears in the g_2 component. This radiation must spread from the central region to the far field, i.e., it must satisfy the Sommerfeld radiation condition

$$\begin{bmatrix} g_1 \\ g_2 \end{bmatrix} \rightarrow \begin{cases} \begin{bmatrix} 0 \\ R_+ e^{-ikx} \end{bmatrix}, & x \gg 1, \\ \begin{bmatrix} 0 \\ R_- e^{ikx} \end{bmatrix}, & x \ll -1, \end{cases} \quad (30)$$

where $k = \sqrt{2\omega - \mu_0}$ is the wavenumber of large- x radiation with frequency 2ω , and R_{\pm} are constants which measure the radiation amplitudes at large- x . A consequence of the Sommerfeld radiation condition is that the resulting solution $[g_1, g_2]^T$ is complex and nonlocal, and this solution can be uniquely determined by various methods [27, 26].

After the U_2 solution (27) is obtained, we now proceed to the U_3 equation at order ϵ^3 . This U_3 equation is

$$\begin{aligned} & (i\partial_t + \partial_{xx} - \mu_0 - V + 2\sigma u_0^2)U_3 + \sigma u_0^2 U_3^* \\ &= \mu_1 U_1 + \mu_2 u_0 - iU_{2T} \\ & - \sigma (2u_0 U_1 U_2 + 2u_0 U_1^* U_2 + 2u_0 U_1 U_2^* + |U_1|^2 U_1). \end{aligned} \quad (31)$$

Inserting the U_1 and U_2 formulae (24) and (27), this U_3 equation reduces to

$$\begin{aligned} & (i\partial_t + \partial_{xx} - \mu_0 - V + 2\sigma u_0^2)U_3 + \sigma u_0^2 U_3^* \\ &= Q_0 + Q_1 e^{i\omega t} + Q_2^* e^{-i\omega t} + Q_3 e^{2i\omega t} + Q_4^* e^{-2i\omega t} \\ & + Q_5 e^{3i\omega t} + Q_6^* e^{-3i\omega t}, \end{aligned} \quad (32)$$

where

$$\begin{aligned}
Q_0 = & -i [\mu_{1T}u_{\mu 0} - \sigma h(|B|^2)_T] \\
& -2\sigma u_0 [iBB_T^*(\psi_1\phi_1 + \psi_2\phi_2 + \psi_1\phi_2) \\
& -iB^*B_T(\psi_1\phi_1 + \psi_2\phi_2 + \psi_2\phi_1)], \tag{33}
\end{aligned}$$

$$\begin{aligned}
Q_1 = & \mu_1 B [\psi_1 - 2\sigma u_0 u_{\mu 0} (2\psi_1 + \psi_2)] - B_{TT}\phi_1 \\
& -\sigma |B|^2 B [\psi_1 (2\psi_2^2 + \psi_1^2) - 2\sigma u_0 h (2\psi_1 + \psi_2) \\
& -2\sigma u_0 (\psi_1 g_1 + \psi_2 g_1 + \psi_2 g_2)], \tag{34}
\end{aligned}$$

$$\begin{aligned}
Q_2 = & \mu_1 B [\psi_2 - 2\sigma u_0 u_{\mu 0} (2\psi_2 + \psi_1)] + B_{TT}\phi_2 \\
& -\sigma |B|^2 B [\psi_2 (2\psi_1^2 + \psi_2^2) - 2\sigma u_0 h (2\psi_2 + \psi_1) \\
& -2\sigma u_0 (\psi_1 g_1 + \psi_1 g_2 + \psi_2 g_2)], \tag{35}
\end{aligned}$$

and Q_3, Q_4, Q_5, Q_6 are functions that are unimportant in our analysis and are thus not shown here. This U_3 solution can be decomposed as

$$\begin{aligned}
U_3(x, t) = & U_{30} + U_{31}e^{i\omega t} + U_{32}e^{-i\omega t} \\
& + U_{33}e^{2i\omega t} + U_{34}e^{-2i\omega t} + U_{35}e^{3i\omega t} + U_{36}e^{-3i\omega t}, \tag{36}
\end{aligned}$$

where

$$L_0 \begin{bmatrix} U_{30} \\ U_{30}^* \end{bmatrix} = \begin{bmatrix} Q_0 \\ -Q_0^* \end{bmatrix}, \tag{37}$$

and

$$(L_0 - \omega) \begin{bmatrix} U_{31} \\ U_{32} \end{bmatrix} = \begin{bmatrix} Q_1 \\ -Q_2 \end{bmatrix}. \tag{38}$$

The Fredholm solvability conditions of the above two equations are that their inhomogeneous terms on the right hand sides be orthogonal to the localized adjoint homogeneous solutions. In view of Eqs. (11) and (16), these solvability conditions are

$$\int_{-\infty}^{\infty} u_0 (Q_0 - Q_0^*) dx = 0, \tag{39}$$

and

$$\int_{-\infty}^{\infty} (\psi_1 Q_1 + \psi_2 Q_2) dx = 0. \tag{40}$$

Inserting the expressions of Q_0, Q_1 and Q_2 above, these solvability conditions lead to the following dynamical equations for the slow variables $\mu_1(T)$ and $B(T)$,

$$\mu_{1T} = \alpha (|B|^2)_T, \tag{41}$$

$$B_{TT} - \beta \mu_1 B + \gamma |B|^2 B = 0, \tag{42}$$

where

$$\alpha = \frac{2\sigma}{P'(\mu_0)} \int_{-\infty}^{\infty} u_0 [h - u_0 (\psi_1 \phi_2 - \psi_2 \phi_1)] dx, \tag{43}$$

$$\beta = \frac{\int_{-\infty}^{\infty} [\psi_1^2 + \psi_2^2 - 4\sigma u_0 u_{\mu_0} (\psi_1^2 + \psi_1 \psi_2 + \psi_2^2)] dx}{\int_{-\infty}^{\infty} (\psi_1 \phi_1 - \psi_2 \phi_2) dx}, \quad (44)$$

and

$$\gamma = \frac{\sigma \int_{-\infty}^{\infty} \left\{ \begin{array}{l} \psi_1^4 + 4\psi_1^2 \psi_2^2 + \psi_2^4 - 4\sigma u_0 h (\psi_1^2 + \psi_1 \psi_2 + \psi_2^2) \\ -2\sigma u_0 [\psi_1^2 g_1 + 2\psi_1 \psi_2 (g_1 + g_2) + \psi_2^2 g_2] \end{array} \right\} dx}{\int_{-\infty}^{\infty} (\psi_1 \phi_1 - \psi_2 \phi_2) dx}. \quad (45)$$

In view of Eq. (13) and our third assumption in the end of Sec. 2, the above three constants are well defined. Dynamical equations (41)-(42) are our normal form for nonlinear wave dynamics near Hamiltonian-Hopf bifurcations in the PDE (1).

Of the three constants in this normal form, α and β are always real. But γ is real only when $2\omega < \mu_0$ and becomes complex if $2\omega > \mu_0$, since the functions (g_1, g_2) involved in the definition of γ are real and complex under those conditions respectively (see earlier text in this section).

The physical meaning of parameter β in Eq. (42) can be revealed by considering small- B solutions. In this case, $\mu_{1T} \approx 0$, i.e., μ_1 is approximately a constant, and the resulting solution (20) is approximately a soliton with propagation constant $\mu \approx \mu_0 + \epsilon^2 \mu_1$. The small perturbation B satisfies $B_{TT} - \beta \mu_1 B \approx 0$, thus $B \sim e^{\tilde{\lambda} t}$, where $\tilde{\lambda} = \pm \epsilon \sqrt{\beta \mu_1}$. If $\beta \mu_1 < 0$, then the perturbation B is bounded, meaning that the soliton is before the Hamiltonian-Hopf bifurcation. When $\beta \mu_1 > 0$, the perturbation B exponentially grows, meaning that the soliton is after the Hamiltonian-Hopf bifurcation. In the latter case, recalling Eq. (24), we see that the quartet of complex eigenvalues born out of Hamiltonian-Hopf bifurcations are $\lambda \approx \pm i\omega \pm \sqrt{\beta(\mu - \mu_0)}$. Thus, physically β determines the growth rate of perturbations after Hamiltonian-Hopf bifurcations.

The normal form (41)-(42) can be further simplified. Notice that Eq. (41) can be integrated once, and we get

$$\mu_1 = \alpha |B|^2 + c_0, \quad (46)$$

where c_0 is a real constant which can be determined from the initial conditions of μ_1 and B . Substituting this equation into (42), we obtain a decoupled equation for B as

$$B_{TT} - \hat{\beta} B + \hat{\gamma} |B|^2 B = 0, \quad (47)$$

where

$$\hat{\beta} = \beta c_0, \quad \hat{\gamma} = \gamma - \alpha \beta. \quad (48)$$

In this equation, $\hat{\beta}$ is a real constant, while $\hat{\gamma}$ can be real or complex depending on the reality of γ . Eq. (47) is a reduced normal form for nonlinear wave dynamics near Hamiltonian-Hopf bifurcations. This reduced normal form is a second-order nonlinear ODE for a complex variable B .

For a different symmetry-breaking bifurcation of solitons in the NLS equation with external potentials (1), a normal form similar to (47) was derived by Pelinovsky and Phan [17], but the variable and the nonlinear coefficient in

their normal form were both real. For the present Hamiltonian-Hopf bifurcation, both the variable B and the nonlinear coefficient $\widehat{\gamma}$ can be complex, and this fact will have important consequences on the solution dynamics, as we will elaborate below.

4 Solution behaviors in the normal form

Now we analyze solution dynamics in the reduced normal form (47).

4.1 Solutions for real nonlinear coefficient $\widehat{\gamma}$

When $\widehat{\gamma}$ is real, Eq. (47) can be solved exactly. In polar variables $B = be^{i\xi}$, where b is the amplitude and ξ the phase of B , Eq. (47) yields

$$b_{TT} - \widehat{\beta}b + \widehat{\gamma}b^3 - \xi_T^2 b = 0, \quad (49)$$

$$(b^2 \xi_T)_T = 0. \quad (50)$$

The second equation shows that

$$b^2 \xi_T = w_0, \quad (51)$$

where w_0 is a real constant. Using this relation, Eq. (49) reduces to

$$b_{TT} - \widehat{\beta}b + \widehat{\gamma}b^3 - \frac{w_0^2}{b^3} = 0, \quad (52)$$

which describes the motion of a particle in a potential well,

$$b_{TT} + W'(b) = 0, \quad (53)$$

where the potential $W(b)$ is

$$W(b) = -\frac{1}{2}\widehat{\beta}b^2 + \frac{1}{4}\widehat{\gamma}b^4 + \frac{w_0^2}{2b^2}. \quad (54)$$

Then depending on system parameters $(\widehat{\beta}, \widehat{\gamma})$ and initial conditions, the solution $B(T)$ can be completely obtained.

A special but important class of solutions arises when $w_0 = 0$, i.e., $\xi_T = 0$. In view of gauge invariance, these solutions are equivalent to real- B solutions, which will be elaborated further below.

When B is real, Eq. (47) becomes

$$B_{TT} - \widehat{\beta}B + \widehat{\gamma}B^3 = 0. \quad (55)$$

The solution dynamics in this equation is best illustrated by its phase portrait in the (B, B_T) plane. Depending on the signs of $\widehat{\beta}$ and $\widehat{\gamma}$, four qualitatively different phase portraits are displayed in Fig. 1. These phase portraits show that when $\widehat{\gamma} > 0$, the trajectories are all bounded and almost always periodic (see the left panels), which correspond to time-periodic bound states (20) in the PDE system (1). When $\widehat{\gamma} < 0$, trajectories all escape to infinity if $\widehat{\beta} > 0$ (upper right panel), and escape to infinity for larger initial conditions and stay bounded and periodic for smaller initial conditions if $\widehat{\beta} < 0$ (lower right panel).

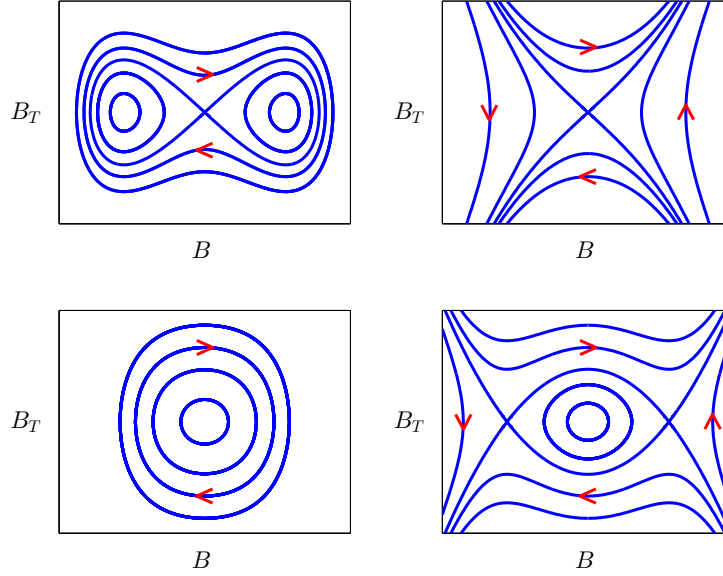


Figure 1: (Color online) Phase portraits of the normal form (47) for real values of $\hat{\gamma}$ and B . Upper left: $\hat{\beta} > 0, \hat{\gamma} > 0$; upper right: $\hat{\beta} > 0, \hat{\gamma} < 0$; lower left: $\hat{\beta} < 0, \hat{\gamma} > 0$; lower right: $\hat{\beta} < 0, \hat{\gamma} < 0$.

4.2 Solutions for complex nonlinear coefficient $\hat{\gamma}$

When $\hat{\gamma}$ is complex, under polar variables $B = be^{i\xi}$ and the notation $w \equiv r^2 \xi_T$, Eq. (47) becomes

$$b_{TT} - \hat{\beta}b + \text{Re}(\hat{\gamma})b^3 - \frac{w^2}{b^3} = 0, \quad (56)$$

$$w_T = -\text{Im}(\hat{\gamma})b^4. \quad (57)$$

The first equation shows that b is bounded away from zero. Then the second equation shows that w keeps increasing or decreasing to infinity. Viewing Eq. (56) as the motion of a particle in a potential well, when w goes to infinity, the potential term $w^2/(2b^2)$ dominates, hence the solution b escapes to infinity as well.

We can further determine precisely in which manner the solution (b, w) escapes to infinity. The nature of nonlinearity in Eqs. (56)-(57) indicates that the solution will escape to infinity in finite time. Suppose the time of blowup is T_0 , and

$$b(T) \sim \frac{b_1}{(T_0 - T)^m}, \quad w(T) \sim \frac{w_1}{(T_0 - T)^n}, \quad T \sim T_0, \quad (58)$$

where b_1, w_1, m, n are real constants to be determined. Substituting these asymptotics into Eq. (57), we get

$$n = 4m - 1, \quad w_1 = -\frac{\text{Im}(\hat{\gamma})b_1^4}{n}. \quad (59)$$

Substituting the asymptotics (58) and the above equation into (56) and using dominant balance, we get

$$m = 1, \quad 2b_1 + \operatorname{Re}(\hat{\gamma})b_1^3 = \frac{w_1^2}{b_1^3}. \quad (60)$$

After solving (b_1, w_1) from the above two equations, we find that the blowup profile of the solution $B(T)$ is

$$b(T) \sim \frac{b_1}{T_0 - T}, \quad \xi(T) \sim c_1 \ln(T_0 - T), \quad T \sim T_0, \quad (61)$$

where

$$b_1 = \frac{3}{\sqrt{2} \operatorname{Im}(\hat{\gamma})} \sqrt{\operatorname{Re}(\hat{\gamma}) + \sqrt{[\operatorname{Re}(\hat{\gamma})]^2 + \frac{8}{9} [\operatorname{Im}(\hat{\gamma})]^2}}, \quad (62)$$

and

$$c_1 = \frac{1}{3} \operatorname{Im}(\hat{\gamma}) b_1^2. \quad (63)$$

Notice that this collapsing profile is completely determined by the nonlinear coefficient $\hat{\gamma}$, except for the collapsing time T_0 . Notice also that both the amplitude b and phase ξ collapse, but at different rates.

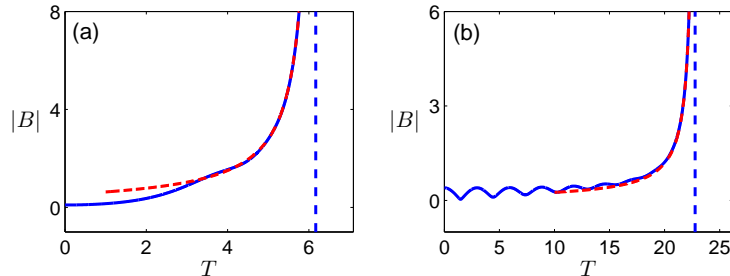


Figure 2: (Color online) Collapsing solutions of the normal form (47) when $\hat{\gamma}$ is complex. (a) $\hat{\beta} = 1$ and $\hat{\gamma} = 1 + i$; (b) $\hat{\beta} = -1$ and $\hat{\gamma} = 1 + i$. Solid blue lines are numerically obtained solutions of the normal form; dashed red lines are analytical collapsing profiles (61); and vertical dashed lines are collapsing times.

To illustrate these collapsing solutions for complex $\hat{\gamma}$, we take $\hat{\gamma} = 1 + i$ and two different values of ± 1 for $\hat{\beta}$. For these parameter choices, we have computed Eq. (47) for various initial conditions and found that the solution always collapses, and the collapsing profile exactly matches that predicted by Eq. (61). Two examples of such computations are displayed in Fig. 2, along with analytical collapsing profiles for comparison. For these two values of $\hat{\beta}$, the two solutions $B(T)$ initially behave quite differently. But they both approach the same collapsing profile (61) in the end.

Collapsing solutions of $B(T)$ correspond to PDE solutions (20) where the Hopf oscillation mode (24) strongly intensifies and the underlying soliton $u_0(x)$ eventually breaks up. This solution collapse occurs when $\hat{\gamma}$ is complex, i.e., when $2\omega > \mu_0$, where resonance with the continuous spectrum arises in the U_2 solution (27). Due to this resonance, energy is channeled from the underlying soliton to the Hopf oscillation mode (24) and continuous-wave radiation. When $2\omega < \mu_0$, this resonance does not occur in U_2 , $\hat{\gamma}$ is real, and the ODE solution $B(T)$ can be bounded (see Fig. 1). However, due to nonlinearity-induced higher harmonics, there always exists a higher harmonic $e^{in\omega}$ for some integer n so that $n\omega > \mu_0$, in which case resonance with the continuous spectrum will occur in the U_n solution of the perturbation expansion (20). As a consequence, when $2\omega < \mu_0$, the B solution is still expected to collapse, and the underlying soliton $u_0(x)$ is still expected to break up, except that these events will take much longer time to develop since the resonance is at higher orders of the perturbation expansion.

5 Numerical examples

In this section, we use several numerical examples to illustrate the theory and compare the numerical results with the normal-form's predictions.

Example 1 In our first example, we take

$$V(x) = -3 [\operatorname{sech}^2(x+1) + \operatorname{sech}^2(x-1)], \quad (64)$$

which is a symmetric double-well potential, and $\sigma = 1$ (focusing nonlinearity). This potential is displayed in Fig. 3(a). This potential admits three linear discrete eigenvalues $\mu_a < \mu_b < \mu_c$, with the middle one $\mu_b \approx 1.4104$. From this linear eigenmode, a family of dipole-type solitons bifurcates out. The reason for choosing this dipole-soliton family bifurcated from the middle linear eigenmode is that, at low amplitudes of these solitons, it can be readily shown that the linear-stability operator iL has two purely imaginary eigenvalues of opposite Krein signatures in the upper half plane. Specifically, one imaginary eigenvalue is approximately $i(\mu_c - \mu_b)$ and it has negative Krein signature, and the other imaginary eigenvalue is approximately $i(\mu_b - \mu_a)$ and it has positive Krein signature. The presence of these two imaginary eigenvalues of opposite Krein signatures makes Hamiltonian-Hopf bifurcation possible as the amplitude of the soliton increases (see Sec. 2).

In Fig. 3(d) the power curve of this soliton family is displayed. At two marked points of this power curve where $\mu = \mu_0 \pm 0.05$, profiles of the solitons are plotted in Fig. 3(b,c). Linear-stability spectra of these solitons are shown in Fig. 3(e,f). It is seen that for the lower-power soliton [see panel (b)], the spectrum is all-imaginary with a pair of discrete imaginary eigenvalues close to each other in the upper half plane [see panel (e)]. This pair of imaginary eigenvalues originate from the eigenvalues $i(\mu_c - \mu_b)$ and $i(\mu_b - \mu_a)$ of zero-power solitons and thus have opposite Krein signatures. For the higher-power soliton [see panel (c)], this pair of discrete eigenvalues have collided and bifurcated off the imaginary axis, indicating that a Hamiltonian-Hopf bifurcation has occurred [see panel

(f)]. The exact location of this Hamiltonian-Hopf bifurcation is at $\mu_0 \approx 1.8572$, where the two discrete eigenvalues coalesce at $i\omega$, with $\omega \approx 1.3450$. Notice that $2\omega > \mu_0$, thus γ is complex. Numerical values for constants α, β and γ in the normal form (41)-(42) are found to be

$$\alpha \approx 0.2660, \quad \beta \approx 0.0476, \quad \gamma \approx 0.0780 + 0.0144i. \quad (65)$$

In obtaining these numbers, the eigenfunction $[\psi_1, \psi_2]^T$ is normalized so that the maximum of $\psi_1^2 + \psi_2^2$ is one.

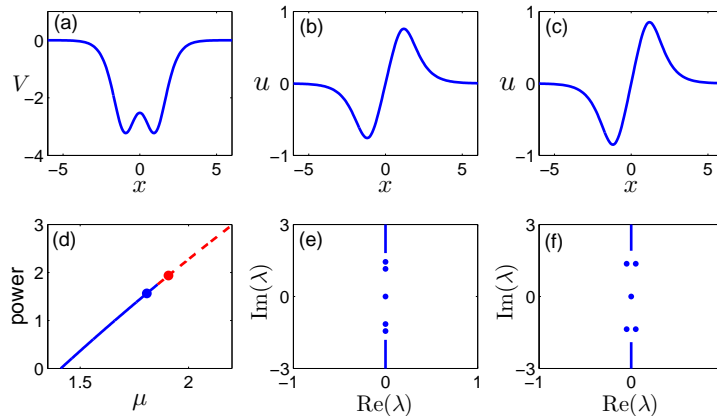


Figure 3: (Color online) Solitons and their stability spectra in Example 1. (a) the double-well potential (64); (b, c) profiles of dipole solitons at the marked blue and red points of the power curve in (d) respectively; blue color of the power curve represents stable solitons, and red color represents unstable solitons; (e, f) linear-stability spectra of the solitons in (b,c) respectively.

Now we numerically investigate the dynamics of solutions near this Hamiltonian-Hopf bifurcation point. First we consider dynamics above the bifurcation. For this purpose, we take the initial condition of the PDE as a perturbation of the unstable soliton in Fig. 3(c) by Hopf oscillation mode (24), corresponding to $\epsilon^2 \mu_1|_{t=0} = 0.05$ and $\epsilon B|_{t=0} = 0.01$ in the perturbation solution (20). Whole-field evolution of this initial condition is illustrated in Fig. 4(a), and the amplitude evolution at $x = 1.2$ is shown Fig. 4(b). It is seen that the underlying soliton breaks up and the solution evolves into oscillations which grow stronger over time. Taking the initial condition of the normal form (47) corresponding to the above initial condition of the PDE, the solution B of the normal form is plotted in Fig. 4(c). This B solution grows and eventually blows up in finite time (the blow-up part is not shown since the perturbation theory will be invalid when the blow-up occurs). Using this B solution, we have reconstructed the perturbation solution (20) (up to order ϵ^2), and the amplitude evolution at $x = 1.2$ is shown Fig. 4(d). Comparing this analytically reconstructed amplitude evolution with the numerical one in panel (b), we can see that the normal form

(47) gives a good qualitative and quantitative prediction of the PDE dynamics above Hamiltonian-Hopf bifurcations over a long period of time.

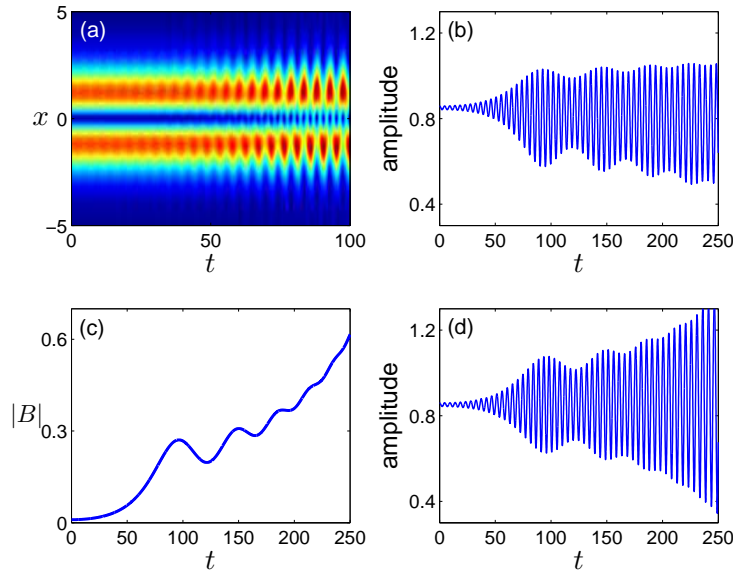


Figure 4: (Color online) Solution evolution above Hamiltonian-Hopf bifurcation in Example 1. (a) Contour plot of the PDE solution in the (x, t) plane; (b) amplitude evolution of the PDE solution versus time. Here the amplitude is measured as $|U(x, t)|$ at location $x = 1.2$; (c) the solution $|B|$ obtained from the normal form (47); (d) amplitude evolution of the analytically reconstructed perturbation solution (20).

Next we consider solution dynamics in Example 1 below the Hamiltonian-Hopf bifurcation. For this purpose, we take the initial condition of the PDE as a perturbation of the stable soliton in Fig. 3(b) by Hopf oscillation mode (24), corresponding to $\epsilon^2 \mu_1|_{t=0} = -0.05$ and $\epsilon B|_{t=0} = 0.08$ in the perturbation solution (20). Evolution of this initial condition is illustrated in Fig. 5(a,b,c). It is seen that the soliton eventually also breaks up due to growing oscillations. This instability is interesting since the underlying soliton is linearly stable [see Fig. 3(e)]. Thus this instability is a nonlinear instability. The analytical reason for this nonlinear instability is that the nonlinear coefficient $\hat{\gamma}$ in the normal form (47) is complex [see Eq. (65)], thus the ODE solution B always collapses both below and above the Hamiltonian-Hopf bifurcation (see Fig. 2). From the ODE solution of the normal form (47), we have also reconstructed the perturbation solution (20), and the amplitude evolution at $x = 1.2$ is shown Fig. 5(d). In this case, the normal form also gives a good qualitative and quantitative prediction of the PDE dynamics over long times.

It should be noticed that even though solitons in Example 1 break up both below and above the Hamiltonian-Hopf bifurcation, this breakup occurs much

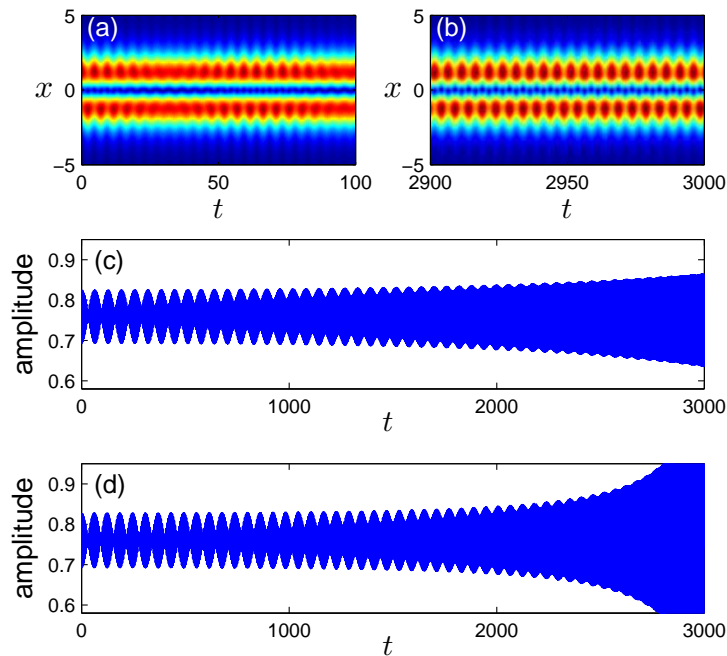


Figure 5: (Color online) Solution evolution below Hamiltonian-Hopf bifurcation in Example 1. (a,b) Contour plots of the PDE solution in the (x, t) plane on smaller and larger time intervals; (c) amplitude evolution of the PDE solution versus time, where the amplitude is measured as $|U(x, t)|$ at location $x = 1.2$; (d) amplitude evolution of the analytically reconstructed perturbation solution (20). In (c,d), seemingly solid blue regions actually comprise of very fast oscillations as in Fig. 4(b,d).

more quickly above the bifurcation point since the soliton in this case is linearly unstable.

Example 2 Our second example pertains to the case where at the Hamiltonian-Hopf bifurcation point, $2\omega < \mu_0$, hence γ is real. In this example, we take

$$V(x) = -3 [\operatorname{sech}^2(x + 1.25) + \operatorname{sech}^2(x - 1.25)], \quad (66)$$

which is a slightly further-separated double-well potential [shown in Fig. 6(a)], and $\sigma = 1$ (focusing nonlinearity). This linear potential also admits three discrete eigenvalues, and the power curve of dipole-type solitons bifurcated from the middle eigenmode is plotted in Fig. 6(b). At the propagation constant $\mu_0 \approx 3.5562$, a Hamiltonian-Hopf bifurcation occurs, and the coalesced eigenvalues on the imaginary axis are $i\omega$, where $\omega \approx 1.5559$. Notice that $2\omega < \mu_0$, thus resonance does not occur in the U_2 solution and γ is real in the normal form (41)-(42). Specifically the constants in the normal form for this second example

are

$$\alpha \approx 0.0372, \quad \beta \approx 0.0263, \quad \gamma \approx 0.2763, \quad (67)$$

where the eigenfunction $[\psi_1, \psi_2]^T$ is normalized to have unit maximum in $\psi_1^2 + \psi_2^2$. In this case, $\hat{\gamma} = \gamma - \alpha\beta > 0$, thus solutions of the normal form (47) are periodic (see Fig. 1).

At the propagation constant $\mu = \mu_0 + 0.05$ [marked by a red dot in Fig. 6(b)], the linear-stability spectrum of the soliton is displayed in Fig. 6(c). The presence of a quartet of complex eigenvalues in this spectrum signals that this soliton is above the Hamiltonian-Hopf bifurcation point.

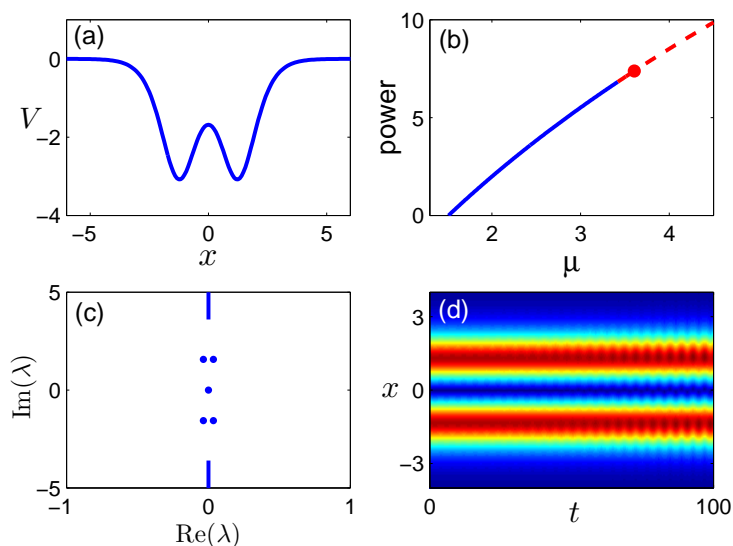


Figure 6: (Color online) (a) The double-well potential (66) in Example 2; (b) power curve of dipole-solitons in this potential, where blue indicates stable solitons and red indicates unstable ones; (c) linear-stability spectrum of the unstable soliton marked by a red dot in panel (b); (d) initial evolution of the unstable soliton at the red dot of panel (b) under perturbations.

Now we perturb this unstable soliton by Hopf oscillation mode (24), corresponding to $\epsilon^2 \mu_1|_{t=0} = 0.05$ and $\epsilon B|_{t=0} = 0.01$ in the perturbation solution (20). The initial evolution of this perturbed state is shown in Fig. 6(d), where the instability is seen to develop. Longer-time amplitude evolution of this perturbed state is plotted in Fig. 7(a), where the amplitude of the solution is measured as $|U(x, t)|$ at location $x = 1.35$. It is seen that the envelope of this amplitude evolves quasi-periodically over a long time, but gradually loses its periodicity in analogy with that in Fig. 5(c) for Example 1. Comparatively the amplitude evolution of analytically reconstructed perturbation solution (20) is displayed in Fig. 7(b). The envelope of this analytical amplitude evolution is periodic, because for this second example, $\hat{\gamma}$ is real, $\hat{\beta} > 0$, and $\hat{\gamma} > 0$, hence the normal

form's solutions are periodic [see Fig. 1 (upper left panel)]. The numerical and analytical amplitude evolutions in Fig. 7 are in good agreement over long times (on the order of hundreds of time units). Their difference over very long times (on the order of thousands of time units) is due to the fact that for the present parameters, $3\omega > \mu_0$, thus resonance with the continuous spectrum will occur in the U_3 solution, and this resonance will break the periodic oscillation. But our perturbation theory and the resulting normal form do not account for resonance at such high orders.

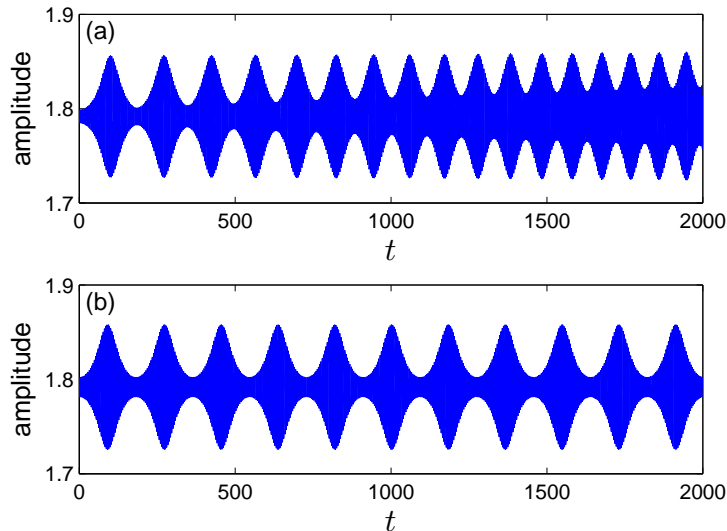


Figure 7: (Color online) (a) Amplitude evolution of the PDE solution for the perturbed soliton in Fig. 6(d) over longer times in Example 2; (b) amplitude evolution of the analytically reconstructed perturbation solution (20).

6 Summary and discussion

In this paper, we have derived a normal form for general Hamiltonian-Hopf bifurcations of solitons in NLS equations with external potentials. This normal form is a simple second-order nonlinear ODE whose dynamics is analytically predictable, and it is asymptotically accurate in describing solution dynamics near Hamiltonian-Hopf bifurcations. We showed that when the nonlinear coefficient in this normal form is complex, which occurs if the second harmonic of the Hopf bifurcation frequency is resonant with the continuous spectrum of the system, the solution of this normal form blows up to infinity in finite time, indicating that solution oscillations near Hamiltonian-Hopf bifurcations will strongly amplify and eventually get destroyed. When the nonlinear coefficient of the normal form is real, the normal form can admit periodic solutions, which correspond

to long-lasting solution oscillations in the original PDE system. Quantitative comparison between the normal form's predictions and true PDE solutions was also made in several numerical examples, and good agreement was obtained. The normal form we derived sheds much light on the analytical understanding of solution behaviors around general Hamiltonian-Hopf bifurcations.

It is noted that even though the normal form in this article was derived for the specific NLS equation (1) with cubic nonlinearity and linear potentials, the same calculation can be trivially extended to generalized NLS equations with arbitrary forms of nonlinearities and potentials (including nonlinear potentials) [19]. Thus the normal form we derived is valid for Hamiltonian-Hopf bifurcations in all generalized nonlinear Schrödinger equations.

It is interesting to notice that our normal form can be dissipative (since its nonlinear coefficient can be complex), even though the original PDE system (1) is conservative. This dissipative nature of the normal form is caused by resonant radiation emission from nonlinearity-induced higher harmonics of oscillating modes. However, this resonant radiation emission does not lead to the decay of solution oscillations. Instead, solution oscillations intensity, as the normal form predicts and the numerics confirms. This situation is analogous to oscillations induced by an internal mode with negative Krein signature [28].

Lastly, we would like to point out that our normal form does not admit chaotic solutions, which indicates that solution dynamics near Hamiltonian-Hopf bifurcations is not chaotic in the PDE system (at least on the time scale of ϵ^{-1} for which the normal form was derived). This analytical prediction is consistent with our numerical PDE results. In the NLS equation with a triple-well potential studied in [15], chaotic motion was reported in both the ODE model and PDE system. In that case, the Hamiltonian-Hopf bifurcation occurred at low powers of solitons, where the chaotic motion was very weak in the ODE model (if at all). Notice that the ODE model derived in [15] did not account for resonant radiation emission of oscillating solutions, thus in the PDE system where such resonant radiation is present, weak chaotic motion of the ODE model may not materialize. Whether there is chaotic motion near Hamiltonian-Hopf bifurcations in the PDE system, on time scales much longer than $O(\epsilon^{-1})$, is a question which may merit further investigation.

Acknowledgment

This work was supported in part by the Air Force Office of Scientific Research (Grant No. USAF 9550-12-1-0244) and the National Science Foundation (Grant No. DMS-1311730).

References

- [1] G. Nicolis and J. F. G. Auchmuty, "Dissipative Structures, Catastrophes, and Pattern Formation: A Bifurcation Analysis", Proc. Natl. Acad. Sci.

- USA 71, 27482751 (1974).
- [2] J.F.G. Auchmuty and G. Nicolis, “Bifurcation analysis of reaction-diffusion equations III. Chemical oscillations”, *Bull. Math. Biol.* 38, 325-350 (1976).
 - [3] R.J. Deissler and H.R. Brand, “Periodic, quasiperiodic, and chaotic localized solutions of the quintic complex Ginzburg-Landau equation”, *Phys. Rev. Lett.* 72, 478481 (1994).
 - [4] A. Ankiewicz, N. Akhmedieva, J.M. Soto-Crespo, “Novel bifurcation phenomena for solitons in nonlinear saturable couplers”, *Optics Communications* 116, 411-415 (1995).
 - [5] B. Buffoni, A. R. Champneys, and J. F. Toland, “Bifurcation and coalescence of a plethora of homoclinic orbits for a Hamiltonian system,” *J. Dyn. Differ. Equ.* 8, 221 (1996).
 - [6] T.S. Yang and T.R. Akylas, “On asymmetric gravity-capillary solitary waves.” *J. Fluid Mech.* 30, 215 (1997).
 - [7] A.V. Getling, *Rayleigh-Bénard Convection: Structures and Dynamics* (World Scientific, Singapore, 1998).
 - [8] A.M. Rucklidge, M. Silber, and J. Fineberg, “Secondary instabilities of hexagons: A bifurcation analysis of experimentally observed Faraday wave patterns”, In J. Buescu, S. Castro, A.P. Dias, and I. Labouriau, editors, *Bifurcations, Symmetry and Patterns*, pp 101-114 (Birkhauser Verlag Basel, Switzerland, 2002).
 - [9] P. G. Kevrekidis, Z. Chen, B. A. Malomed, D. J. Frantzeskakis, and M. I. Weinstein, “Spontaneous symmetry breaking in photonic lattices: Theory and experiment”, *Phys. Lett. A* 340, 275-280 (2005).
 - [10] T. Kapitula, P. G. Kevrekidis, and Z. Chen, “Three is a crowd: Solitary waves in photorefractive media with three potential wells”, *SIAM J. Appl. Dyn. Syst.* 5, 598-633 (2006).
 - [11] E.W. Kirr, P.G. Kevrekidis, E. Shlizerman, and M.I. Weinstein, “Symmetry-breaking bifurcation in nonlinear Schrödinger/Gross-Pitaevskii equations”, *SIAM J. Math. Anal.* 40, 56604 (2008).
 - [12] C. Wang, G. Theocharis, P.G. Kevrekidis, N. Whitaker, K.J.H. Law, D.J. Frantzeskakis, and B.A. Malomed, “Two-dimensional paradigm for symmetry breaking: The nonlinear Schrödinger equation with a four-well potential”, *Phys. Rev. E* 80, 046611 (2009).
 - [13] J.L. Marzuola and M.I. Weinstein, “Long time dynamics near the symmetry breaking bifurcation for nonlinear Schrödinger/Gross-Pitaevskii equations”, *Discrete and Continuous Dyn. Syst. A* 28, 1505-1554 (2010).
 - [14] E.W. Kirr, P.G. Kevrekidis, and D.E. Pelinovsky, “Symmetry-breaking bifurcation in the nonlinear Schrödinger equation with symmetric potentials”, *Commun. Math. Phys.* 308, 795844 (2011).
 - [15] R.H. Goodman, “Hamiltonian Hopf bifurcations and dynamics of NLS/GP standing-wave modes”, *J. Phys. A* 44, 425101 (2011).
 - [16] H.C. Kao and E. Knobloch, “Weakly subcritical stationary patterns. Eckhaus instability and homoclinic snaking”, *Phys. Rev. E* 85 026211 (2012).

- [17] D.E. Pelinovsky and T. Phan, “Normal form for the symmetry-breaking bifurcation in the nonlinear Schrodinger equation”, *J. Differential Equations* 253, 27962824 (2012).
- [18] J. Yang, “No Stability Switching at Saddle-Node Bifurcations of Solitary Waves in Generalized Nonlinear Schroedinger Equations”, *Phys. Rev. E* 85, 037602 (2012).
- [19] J. Yang, “Classification of solitary wave bifurcations in generalized nonlinear Schrödinger equations”, *Stud. Appl. Math.* 129, 133-162 (2012).
- [20] J. Yang, “Stability analysis for pitchfork bifurcations of solitary waves in generalized nonlinear Schroedinger equations”, *Physica D* 244, 50-67 (2013).
- [21] R. S. MacKay, “Stability of equilibria of Hamiltonian systems,” in *Hamiltonian Dynamical Systems*, edited by R. S. MacKay and J. Meiss (Adam Hilger, Bristol, 1987), pp. 137-153.
- [22] D. E. Pelinovsky, *Localization in Periodic Potentials: From Schrödinger Operators to the Gross-Pitaevskii Equation* (Cambridge University Press, New York, 2011).
- [23] T. Kapitula and K. Promislow, *Spectral and Dynamical Stability of Nonlinear Waves* (Springer, Berlin, 2013).
- [24] Y. S. Kivshar and G. P. Agrawal, *Optical Solitons: From Fibers to Photonic Crystals* (Academic Press, San Diego, 2003).
- [25] L.P. Pitaevskii and S. Stringari, *Bose-Einstein Condensation* (Oxford University Press, Oxford, 2003).
- [26] J. Yang, *Nonlinear Waves in Integrable and Nonintegrable Systems* (SIAM, Philadelphia, 2010).
- [27] D.E. Pelinovsky and J. Yang, “A normal form for nonlinear resonance of embedded solitons.” *Proc. Roy. Soc. Lond. A.* 458, 1469-1497 (2002).
- [28] P.G. Kevrekidis, D.E. Pelinovsky, and A. Saxena, “When linear stability does not exclude nonlinear instability”, *Phys. Rev. Lett.* 114, 214101 (2015).